Research Article **Open Access**

Aranka Derzsi*, Edmund Schüngel, Zoltán Donkó, Julian Schulze

Electron heating modes and frequency coupling effects in dual-frequency capacitive CF_4 plasmas

Abstract: Two types of capacitive dual-frequency discharges, used in plasma processing applications to achieve the separate control of the ion flux, Γ_i, and the mean ion energy, $\langle E_i \rangle$, at the electrodes, operated in CF_4, are investigated by particle-in-cell simulations: (i) In classical dual-frequency discharges, driven by significantly different frequencies (1.937 MHz + 27.12 MHz), $\langle E_i \rangle$ and Γ_i are controlled by the voltage amplitudes of the low-frequency and high-frequeny components, Φ_{LF} and Φ_{HF}, respectively. (ii) In electrically asymmetric (EA) discharges, operated at a fundamental frequency and its second harmonic (13.56 MHz + 27.12 MHz), Φ_{LF} and Φ_{HF} control Γ_i, whereas the phase shift between the driving frequencies, θ, is varied to adjust $\langle E_i \rangle$.

We focus on the effect of changing the control parameter for $\langle E_i \rangle$ on the electron heating and ionization dynamics and on Γ_i. We find that in both types of dual-frequency strongly electronegative discharges, changing the control parameter results in a complex effect on the electron heating and ionization dynamics: in classical dual-frequency discharges, besides the frequency coupling affecting the sheath expansion heating, additional frequency coupling mechanisms influence the electron heating in the plasma bulk and at the collapsing sheath edge; in EA dual-frequency discharges the electron heating in the bulk results in asymmetric ionization dynamics for values of θ around 45°, *i.e.*, in the case of a symmetric applied voltage waveform, that affects the dc self-bias generation.

Keywords: dual-frequency RF discharges, electronegative plasmas, electrical asymmetry effect, frequency-coupling effects, electron heating modes

***Corresponding author: Aranka Derzsi:** Institute for Solid State Physics and Optics, Wigner Research Centre for Physics, Hungarian Academy of Sciences, 1121 Budapest, Hungary, E-mail: derzsi.aranka@wigner.mta.hu
Zoltán Donkó: Institute for Solid State Physics and Optics, Wigner Research Centre for Physics, Hungarian Academy of Sciences, 1121 Budapest, Hungary
Edmund Schüngel, Julian Schulze: Department of Physics, West Virginia University, Morgantown, WV 26506, USA

DOI: 10.1515/chem-2015-0044
received January 31, 2014; accepted April 3, 2014.

1 Introduction

Capacitively coupled radio frequency (CCRF) discharges are widely used for a variety of applications: they are basic tools in plasma enhanced chemical vapor deposition (PECVD) and plasma etching, in the semiconductor industry and in the field of surface processing of medical interest [1,2]. In such applications complex mixtures of reactive, often electronegative, gases are required, for instance carbon-tetrafluoride (CF_4), which is frequently used to etch silicon and silicon-dioxide. CF_4 discharges exhibit a complex chemistry and become strongly electronegative under typical operating conditions. Under these conditions the plasma composition, the electron heating and ionization dynamics, and the discharge operation differ significantly from those of electropositive discharges [3-20].

Low-pressure electropositive discharges operate either in an α–mode [21] (at low pressures and driving voltages), where the ionization is dominated by electrons accelerated by the oscillating sheaths and the field reversals during sheath collapse [22-26], or in a γ-mode [21] (at high pressures and/or voltages), where the ionization is dominated by secondary electron avalanches inside the sheaths at times of high sheath voltage. In these discharge operation modes the electron heating and ionization rates are typically high around the sheath edges and low in the plasma bulk. Transitions between these modes are induced by changing the pressure and/or voltage [21]. At very high pressures, *e.g.* in atmospheric pressure microplasmas, the ionization can be dominated by ohmic heating in the bulk. In this Ω–mode [27], a high electric field builds up in the bulk region due to the low electrical conductivity caused by the high electron-neutral collision frequency – this drift field accelerates electrons to high energies to create ionization in the bulk. Similar electron heating and ionization dynamics in the bulk region have been found in dusty plasmas [28-30] as well as in discharges operated

in various electronegative gases [7,8,15-19,31-35]. While in case of dust contaminated plasmas the origin of the low electrical conductivity (and that of the high electric field) in the bulk is the loss of charged particles the dust particles, in electronegative plasmas the depleted electron density is due to electron attachment in the discharge center. Further electron heating and ionization mechanisms have been identified in electronegative plasmas [17]: at the collapsing sheath edge ionization is generated by electrons accelerated by an ambipolar field due to local maxima of the electron density in the electropositive edge region of the discharge. The drift-ambipolar (DA) mode, specific to electronegative discharges, refers to the simultaneous presence of both the ohmic heating (Ω–mode) and the heating due to the ambipolar field in electronegative plasmas [17,18]. Transitions between the DA-mode and the α–mode have been found in simulations and experiments [17]: by increasing the pressure at a fixed voltage, a transition from the α–mode to the DA-mode is induced; by increasing the voltage at a fixed pressure, a transition from the DA-mode to the α–mode is observed.

These electron heating dynamics are crucial to both the gas phase chemistry and the properties of the plasma at the surrounding surfaces. The realization of the separate control of the mean ion energy, $\langle E_i \rangle$, and the ion flux, Γ_i, at the electrode surfaces is a central issue in CCRF discharges used in various plasma processing applications. Different methods and discharge configurations, such as hybrid capacitive/inductive discharges [36-41] and dual-frequency discharges [42-45], have been developed to reach this goal. There are two types of capacitive dual-frequency discharges typically used in industrial applications:

(i) In classical dual-frequency discharges one electrode is driven by two substantially different frequencies, *e.g.* 1.937 MHz + 27.12 MHz. The driving voltage waveform is defined as

$$\tilde{\phi}(t) = \phi_{LF} \cos\left(2\pi f_{LF} t\right) + \phi_{HF} \cos\left(2\pi f_{HF} t\right), \quad (1)$$

where Φ_{LF} and Φ_{HF} are the low-frequency (f_{LF}) and high-frequency (f_{HF}) voltage amplitudes, respectively. In such discharges $\langle E_i \rangle$ is controlled by the low-frequency voltage amplitude (by varying the mean sheath voltage), while Γ_i is adjusted by the high-frequency voltage amplitude (due to the enhanced electron heating at high frequencies). However, a coupling effect of the driving frequencies was found to reduce the quality of the separate control of ion properties [46-49], which is further limited by the effect of secondary electrons [50-52].

(ii) Electrically asymmetric (EA) dual-frequency discharges are operated at a fundamental frequency and its second harmonic, *e.g.* 13.56 MHz + 27.12 MHz, with a fixed but adjustable phase shift between the driving harmonics. The driving voltage waveform is defined as

$$\tilde{\phi}(t) = \phi_{LF} \cos\left(2\pi f t + \theta\right) + \phi_{HF} \cos\left(4\pi f t\right), \quad (2)$$

where f is the fundamental frequency and θ is the phase shift between the driving harmonics. In such discharges θ is varied to control the mean ion energy at the electrodes, whereas the voltage amplitudes determining the ion flux are kept constant. Tuning θ, a dc self-bias, η, is generated *via* the Electrical Asymmetry Effect (EAE) [53-70] – this self-bias voltage is almost a linear function of θ. Hence, the mean sheath voltages and $\langle E_i \rangle$ can be controlled separately from Γ_i by adjusting θ.

The quality of the separate control of ion properties has been thoroughly examined in electropositive gases (mainly in argon) for both types of capacitive dual-frequency discharges. It was found that EA discharges allow a significantly better separate control of ion properties compared to classical dual-frequency discharges by eliminating the frequency coupling effects and reducing the negative impact of secondary electrons. Less attention has been paid to the detailed examination of the performance of these dual-frequency discharges in electronegative gases, a feature that is relevant to the applications. Important effects of the specific electron heating and ionization dynamics on the separate control of ion properties in electronegative gases have been recently pointed out [16,18].

Here, we analyze the control of ion properties and its limitations, in both classical and EA dual-frequency discharges in CF_4, *via* self-consistent particle-in-cell simulations. For both types of discharges we perform simulations at different pressures varying the control parameter for the mean ion energy: in classical dual-frequency discharges Φ_{LF} is varied at constant Φ_{HF}; in EA discharges θ is changed at constant $\Phi_{LF}=\Phi_{HF}$. We focus on the effect of the control parameter on the electron heating and ionization dynamics and its influence on the ion flux at the electrodes at different pressures.

The paper is structured in the following way: in the second section we present the details of the simulation method. In the third section, the simulation results are presented and discussed. This section is divided into two parts, one comprising the results obtained for the classical dual-frequency discharges, while the other containing the results obtained for EA discharges. Finally, conclusions are drawn in section four.

2 Calculation details

The simulations are based on a bounded electrostatic particle-in-cell (PIC) code complemented with Monte Carlo treatment of collision processes. This PIC/MCC code, which has been used in a previous study under different conditions [16], is one-dimensional in space and three dimensional in velocity (1D3V). Here, geometrically symmetric dual-frequency discharges are investigated in pure CF_4. The electrodes are considered to be infinite, plane parallel, and separated by a distance of d=1.5 cm. One of the electrodes is grounded, the other is driven by the superposition of two radio frequencies. The gas temperature is 350 K. The ion-induced secondary electron emission coefficient, γ, is set to 0.1, the probability of electron reflection from the electrodes is set to 0.2 based on the data provided in [71].

Simulations are performed for both the classical and the EA dual-frequency discharges at two different pressures (10 Pa and 80 Pa). In case of classical dual-frequency discharges, a voltage waveform is applied according to equation (1): f_{LF} = 1.937 MHz and f_{HF} = 27.12 MHz, Φ_{HF} is kept constant (Φ_{HF}=300 V at 10 Pa and Φ_{HF}=100 V at 80 Pa), and Φ_{LF} is varied. In EA dual-frequency discharges, a voltage waveform, according to equation (2), is used with a fundamental frequency of f=13.56 MHz and simulations are carried out for different phase shifts between the driving harmonics (θ is set to values between 0° and 90°). The voltage amplitudes are equal and constant, $\Phi_{LF}=\Phi_{HF}$=100 V at 10 Pa and $\Phi_{LF}=\Phi_{HF}$=50 V at 80 Pa. We investigate the electron heating and ionization dynamics under various discharge conditions and explore how these dynamics and the ion fluxes at the electrodes are affected by changing the control parameter for the mean ion energy - Φ_{LF} and θ in classical and EA dual-frequency discharges, respectively.

The plasma species traced in the model are electrons, and CF_3^+, CF_3^- and F^- ions, found to be the dominant charged species in previous studies of CF_4 discharges [3-7]. The electron-neutral collision processes taken into account in the model are listed in Table 1, the cross sections for these collisions are taken from [72-74]. The collision processes involving different ions and CF_4 molecules considered in the model are listed in Table 2. These processes are treated according to [3, 75-76]. The ion-ion and electron-ion recombination processes are described based on the procedure of Nanbu and Denpoh [77]. The rate of electron-CF_3^+ recombination is $3.95\times10^{-15}T_i^{-1}T_e^{-0.5}$ $m^3 s^{-1}$, where T_i and T_e are the ion and electron temperatures, respectively, given in eV [8]. In previous studies, the simulation results proved to be largely influenced by the value of the ion-ion

Table 1: List of electron-CF_4 collision processes considered in the model. E_0 is the energy threshold in eV.

Collision type	Product	E_0 [eV]
Elastic momentum transfer		0
Vibrational excitation		0.108
Vibrational excitation		0.168
Vibrational excitation		0.077
Electronic excitation	CF_4^*	7.54
Dissociative ionization	CF_3^{++}	41
Dissociative ionization	CF_3^+	16
Dissociative ionization	CF_2^{++}	42
Dissociative ionization	CF_2^+	21
Dissociative ionization	CF^+	26
Dissociative ionization	C^+	34
Dissociative ionization	F^+	34
Attachment	F^-	0
Attachment	CF_3^-	0
Neutral dissociation	CF_3	12
Neutral dissociation	CF_2	17
Neutral dissociation	CF	18

Table 2: List of ion-CF_4 collision processes considered in the model. E_0 is the energy threshold in eV.

Projectile	Reaction	E_0 [eV]
CF_3^+	$CF_3^+ + CF_4 \rightarrow CF_2^+ + CF_4 + F$	5.843
CF_3^+	$CF_3^+ + CF_4 \rightarrow CF_3^+ + CF_3 + F$	5.621
CF_3^+	$CF_3^+ + CF_4 \rightarrow CF_3^+ + CF_4$	0
CF_3^-	$CF_3^- + CF_4 \rightarrow CF_4 + CF_3 + e^-$	1.871
CF_3^-	$CF_3^- + CF_4 \rightarrow CF_3^- + CF_3 + e^-$	5.621
CF_3^-	$CF_3^- + CF_4 \rightarrow CF_2 + CF_4 + F^-$	1.927
CF_3^-	$CF_3^- + CF_4 \rightarrow CF_3^- + CF_4$	0
F^-	$F^- + CF_4 \rightarrow CF_4 + F + e^-$	3.521
F^-	$F^- + CF_4 \rightarrow CF_3 + F^- + F$	5.621
F^-	$F^- + CF_4 \rightarrow F^- + CF_4$	0

(CF_3^++F, CF_3^++CF_3^-) recombination rate coefficient [6,16,17]. Here, we use the value of 5.5×10^{-13} $m^3 s^{-1}$ taken from [7] that resulted in a good agreement between the simulation and the experiment [17].

3 Results and discussion

3.1 Classical dual-frequency discharges

Fig. 1 shows spatio-temporal plots of the electron heating rate in classical dual-frequency discharges (driven at 1.937 MHz + 27.12 MHz) obtained at 10 Pa (first row) and 80 Pa (second row) for different values of the low-frequency voltage amplitude, Φ_{LF} (first column: Φ_{LF}=0 V, second column: Φ_{LF}=100 V, third column: Φ_{LF}=200 V). The high-frequency voltage amplitude, Φ_{HF}, is 300 V and 100 V at 10 Pa and 80 Pa, respectively. The spatio-temporal distribution of the ionization rate and the electric field corresponding to these cases are shown in Fig. 2 and Fig. 3, respectively. In order to provide a good visibility of the distribution patterns in different spatio-temporal plots, all the graphs cover 258.23 ns on the horizontal axis, corresponding to one half low-frequency period (7 high-frequency periods). The vertical axes show the distance from the powered electrode. The studied (classical dual-frequency) discharges are characterized by a symmetrical discharge structure over the low-frequency period, therefore the discharge properties observed at the powered and grounded electrodes during the first half of the low-frequency period are observed at the grounded and powered electrodes, respectively, during the second half of the given low-frequency period as well. First, we analyze the effect of the variation of the low-frequency voltage amplitude on the electron heating and ionization dynamics defining the discharge operation mode and plasma parameters at different pressures. Second, we discuss the impact of changing Φ_{LF} on the separate control of ion properties at the electrodes under the conditions investigated.

At 10 Pa, for Φ_{LF}=0 V, the spatio-temporal distribution of the electron heating rate (Fig. 1, top left plot) and ionization rate (Fig. 2, top left plot) are dominated by the sheath expansion heating, i.e. the discharge is operated in the α–mode. Moreover, a weak electron heating pattern in the sheaths, due to the acceleration and multiplication of secondary electrons released at the electrode surfaces, is visible. This single-frequency discharge is characterized by an electronegativity of 0.22 (Fig. 5). The electronegativity is defined as the ratio of the negative ion density to the electron density averaged over the electrode gap and

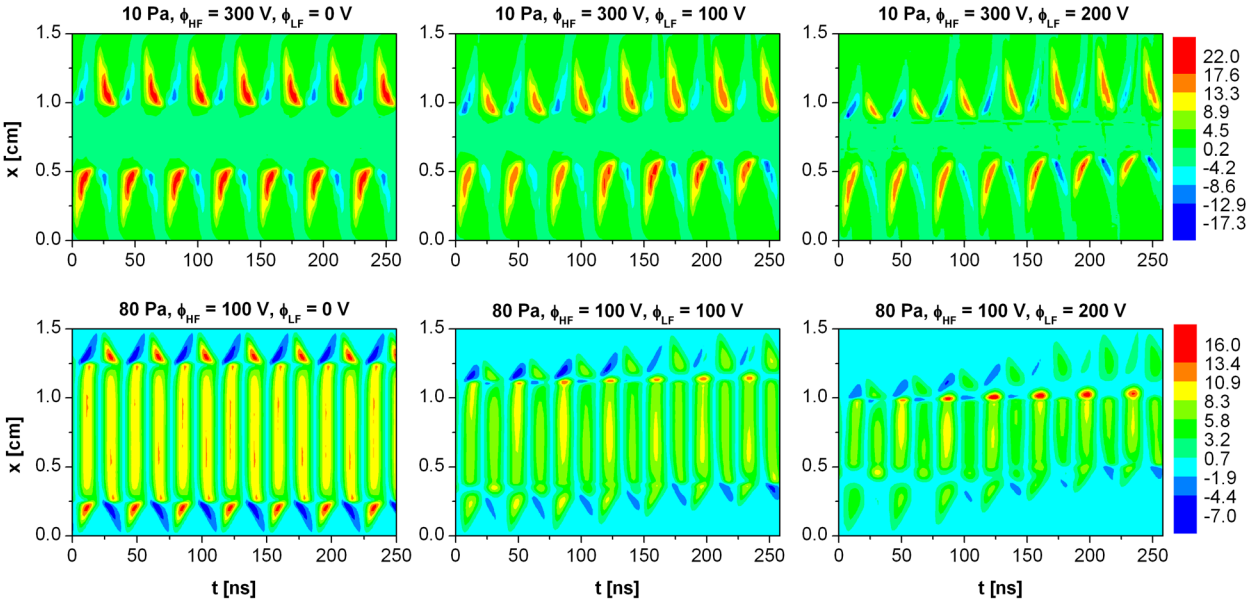

Figure 1: Spatio-temporal distribution of the electron heating rate in classical dual-frequency discharges operated at 1.937 MHz + 27.12 MHz for different values of the low-frequency voltage amplitude, Φ_{LF}, at 10 Pa (first row) and at 80 Pa (second row). First column: Φ_{LF}=0 V. Second column: Φ_{LF}=100 V. Third column: Φ_{LF}=200 V. Φ_{HF}=300 V at 10 Pa. Φ_{HF}=100 V at 80 Pa. The color scales are given in 10^4 Wm^{-3} and apply to all plots in the same row. The horizontal axis corresponds to half of the LF period. The vertical axis shows the distance from the powered electrode.

time. The negative ions are confined within the discharge center (Fig. 4, top left plot) by the sheaths electric field. The electron density is high in the bulk region, ensuring a high bulk conductivity, σ, at low pressures. Due to this, the drift electric field in the discharge center, E=j/σ, is low (Fig. 3, top left plot), since under such conditions a low electric field is sufficient to drive a given RF current, j, trough the plasma bulk [16]. The dc conductivity is defined as $\sigma=(n_e e^2)/(m_e \nu)$, where n_e is the electron density in the bulk, e is the elementary charge, m_e is the mass of electron, and ν is the electron-neutral collision frequency. The electrical properties of the discharge are characterized by the dc conductivity, as the electron collision frequency is well above both applied radio frequencies [1].

When applying a low frequency source (Φ_{LF}>0V) at 10 Pa, the discharge operation mode is not changed compared to the single-frequency case; the electrons causing ionization are again accelerated by the high-frequency sheath oscillations. However, as the high-frequency sheath oscillations are shifted to the regions of higher plasma density at the times of large low-frequency sheath, the electron heating becomes less effective (Fig. 1, top middle and right plots). This frequency-coupling, a well-known effect in electropositive discharges, results in reduced ionization with increasing low-frequency voltage amplitude (Fig. 2, top middle and right plots). It should be noted that the modulation of the ionization by energetic electrons accelerated by the high frequency sheath expansion is much stronger than the modulation of the electron heating. This is due to the fact that more electrons gain less energy when the low frequency sheath is expanded because the plasma density is increasing towards the quasineutral plasma bulk. Accordingly, only a very small fraction of these electrons gains enough energy to overcome the ionization threshold energy. The electronegativity of the discharge increases (but remains low) with increasing Φ_{LF}; it is 0.41 and 1.25 at Φ_{LF}=100 V and Φ_{LF}=200 V, respectively (Fig. 5). The electric field in the discharge center remains low for Φ_{LF}>0V (Fig. 3, top middle and right plots) since conditions for a good conductivity of the bulk are still given under these conditions.

At 80 Pa, for Φ_{LF}=0 V, the single-frequency discharge operates in a hybrid α-DA mode [17]. Besides the sheath expansion heating, significant electron heating in the bulk plasma region and at the collapsing sheath edges can be observed (Fig. 1, bottom left plot) that dominate the ionization dynamics (Fig. 2, bottom left plot). In this case, the electronegativity of the discharge is high (32.5) due to the enhanced electron attachment at high pressures, and the electron density is low in the bulk (Fig. 4, bottom left plot), leading to a low bulk conductivity. Therefore, a high

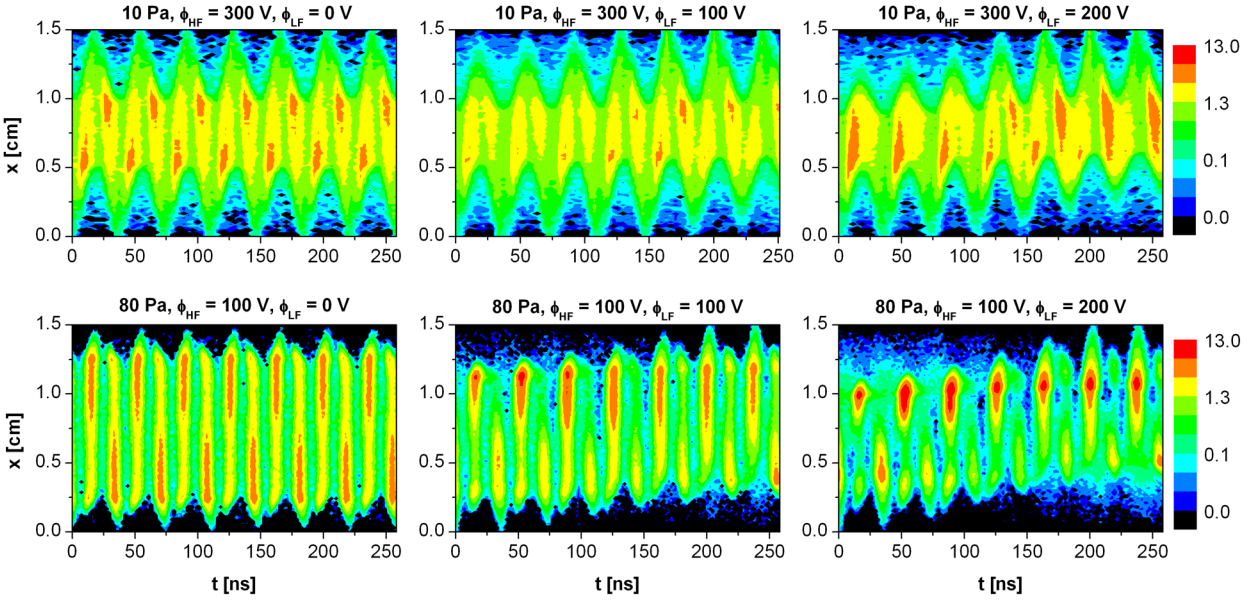

Figure 2: Spatio-temporal distribution of the ionization rate in classical dual-frequency discharges operated at 1.937 MHz + 27.12 MHz for different values of the low-frequency voltage amplitude, Φ_{LF}, at 10 Pa (first row) and at 80 Pa (second row). First column: Φ_{LF}=0 V. Second column: Φ_{LF}=100 V. Third column: Φ_{LF}=200 V. Φ_{HF}=300 V at 10 Pa. Φ_{HF}=100 V at 80 Pa. The color scales, given in 10^{21} $m^{-3}s^{-1}$, are logarithmic, and apply to all plots in the same row. The horizontal axis corresponds to half of the LF period. The vertical axis shows the distance from the powered electrode.

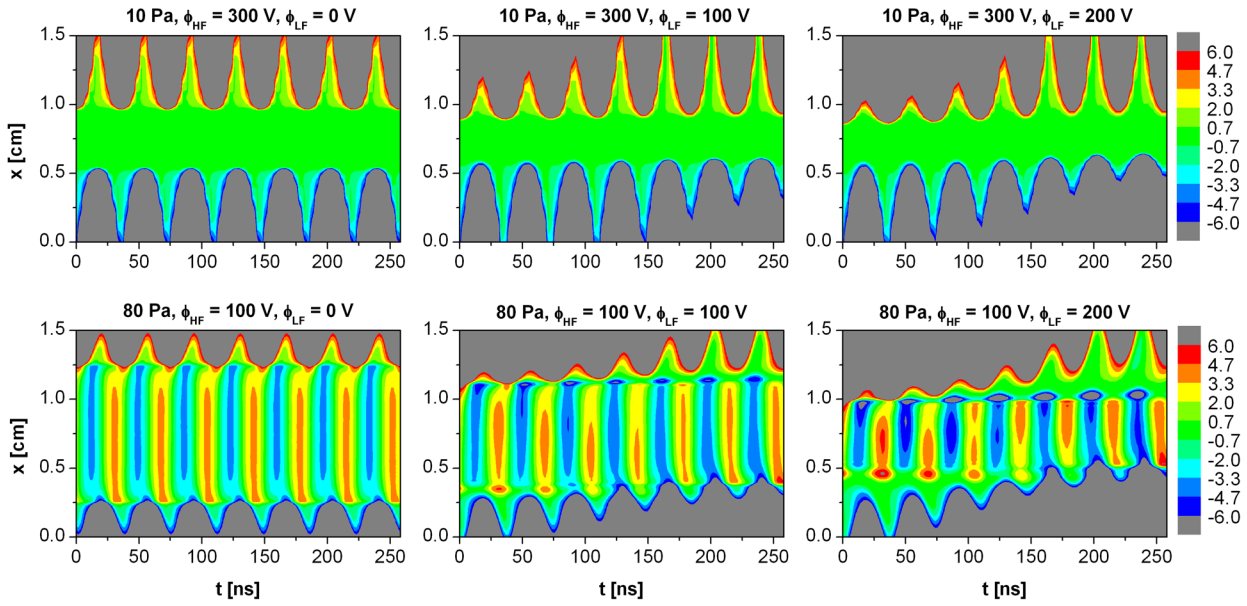

Figure 3: Spatio-temporal distribution of the electric field in classical dual-frequency discharges operated at 1.937 MHz + 27.12 MHz for different values of the low-frequency voltage amplitude, Φ_{LF}, at 10 Pa (first row) and at 80 Pa (second row). First column: Φ_{LF}=0 V. Second column: Φ_{LF}=100 V. Third column: Φ_{LF}=200 V. Φ_{HF}=300 V at 10 Pa. Φ_{HF}=100 V at 80 Pa. The color scales are given in 10^3 Vm^{-1} and apply to all plots in the same row. The horizontal axis corresponds to half of the LF period. The vertical axis shows the distance from the powered electrode.

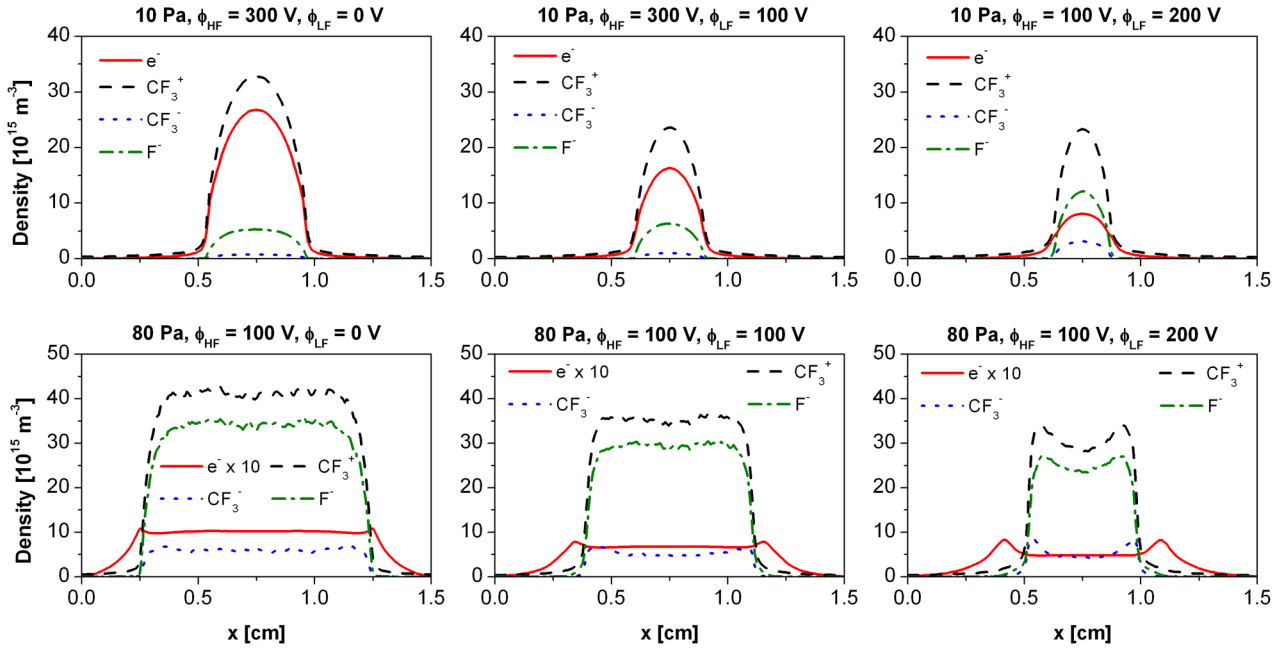

Figure 4: Time averaged charged particle densities in classical dual-frequency discharges operated at 1.937 MHz + 27.12 MHz for different values of the low-frequency voltage amplitude, Φ_{LF}, at 10 Pa (first row) and at 80 Pa (second row). First column: Φ_{LF}=0 V. Second column: Φ_{LF}=100 V. Third column: Φ_{LF}=200 V. Φ_{HF}=300 V at 10 Pa. Φ_{HF}=100 V at 80 Pa.

drift electric field, E=j/σ, builds up in the bulk region, in order to drive a given RF current through the bulk. This electric field accelerates electrons to high energies that cause the ionization in the bulk. A high electric field develops at the collapsing sheath edges as well, that results in additional electron heating and ionization. This ambipolar field, $E=-kT_e/n_e(\partial n_e/\partial x)$, where T_e is the electron temperature and k is the Boltzmann constant, is due to the

high electron density gradient found close to the position of the boundary between the electronegative bulk and electropositive sheath regions. At this position, the electron density peaks in order to ensure quasineutrality (Fig. 4, bottom left plot).

When applying a low-frequency source at 80 Pa, strong electron heating and ionization in the bulk can be observed at phases when both the low-frequency and high-frequency sources accelerate electrons towards the same electrode (Figs. 1 and 2, top middle and right plots): during the first half of the low-frequency period, the low-frequency sheath expands at the powered electrode; at the times of high-frequency sheath expansion both sources generate electron currents directed towards the grounded electrode. The electron current density, j, is high at these phases, while it is low at the times of high-frequency sheath collapse in the first half of the low-frequency period, when the electron accelerations, due to the two different sources, are opposed to each other. Here, the electronegativity is 36 and 28 at Φ_{LF}=100 V and Φ_{LF}=200 V, respectively (Fig. 5). Hence, the bulk conductivity is low due to the depleted electron density (Fig. 4, bottom middle and right plots). The strength of the drift electric field, E=j/σ, varies temporally according to j, *i.e.*, it is high at the phases when the electron acceleration of both sources have the same direction and it is low at the phases when the effect of the sources on the electron motion is opposed (Fig. 3, top middle and right plots). During the second half of the low-frequency period (not shown in the spatio-temporal plots), when the low-frequency sheath adjacent to the powered electrode collapses, the interaction of the sources has similar effects on the electron heating and ionization dynamics as during the first half of the period; the difference is that the sources cause electrons to be accelerated in the same direction (towards the powered electrode) at the times of high-frequency sheath collapse at the bottom electrode and in opposite directions at the times of high-frequency sheath expansion.

The electron heating and ionization due to ambipolar electric fields at the collapsing high-frequency sheath edge are also affected by the low-frequency source. At the phases of maximum sheath length in the low-frequency period, the positions of the electron density peaks at the boundary of the electronegative bulk and the electropositive sheath region can be covered by the sheath. At these times, the electrons are repelled from the adjacent electrodes towards the discharge center from these positions by the sheath electric field, this way the local electron density maxima are removed. At these phases, the conditions required for the development

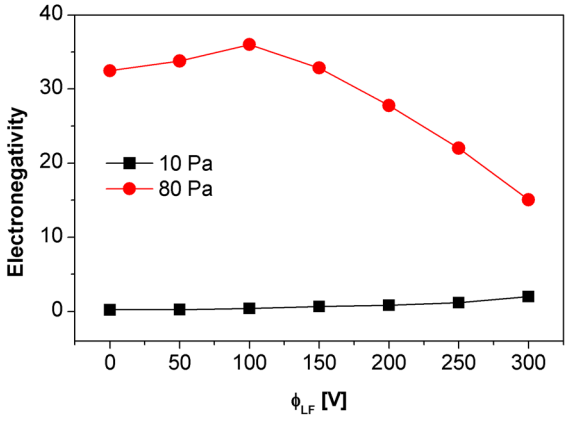

Figure 5: Electronegativity of classical dual-frequency discharges, operated at 1.937 MHz + 27.12 MHz, as a function of the low-frequency voltage amplitude, Φ_{LF}, at different pressures (10 Pa and 80 Pa). Φ_{HF}=300 V at 10 Pa and Φ_{HF}=100 V at 80 Pa.

of ambipolar electric fields are not fulfilled. Therefore, electron heating and ionization, due to ambipolar electric fields at the collapsing high-frequency sheath edge of a given electrode, is only possible when the sheath is small and the positions of the electron density maxima are not covered by the sheath. Nevertheless, the distinct peaks of the electron heating (Fig. 1) due to the ambipolar electric field (Fig. 3) dominate the ionization pattern (Fig. 2) in the dual-frequency high pressure plasma, so that the strong localization of this main ion source leads to a convex shaped ion diffusion profile in the plasma bulk region (Fig. 4). In general, this ambipolar heating mode is enhanced by a frequency coupling effect, which is only present in electronegative plasmas: The diffusion of negative ions across the maximum extensions of the two sheaths is possible due to the relatively long period of the low frequency voltage component, which leads to a long period of sheath collapse within one lf period. This reduces the electron density close to the maximum sheath edge, since quasineutrality must be ensured at these positions at the times of sheath collapse. Moreover, close to the maximum sheath edge positive ions are accelerated towards the electrode less strongly compared to the single frequency scenario, since this region is outside of the momentary sheath for a longer time within one lf period. Thus, the positive ion density gradient is weaker close to the maximum sheath edge compared to the single frequency case. Thus, in the electropositive edge region the local maximum of the electron density is more pronounced in the dual-frequency case compared to the single-frequency one. This leads to a stronger local gradient of the electron density (Fig. 4), a stronger ambipolar electric field (Fig. 3), and stronger electron heating (Fig. 1) at the times when

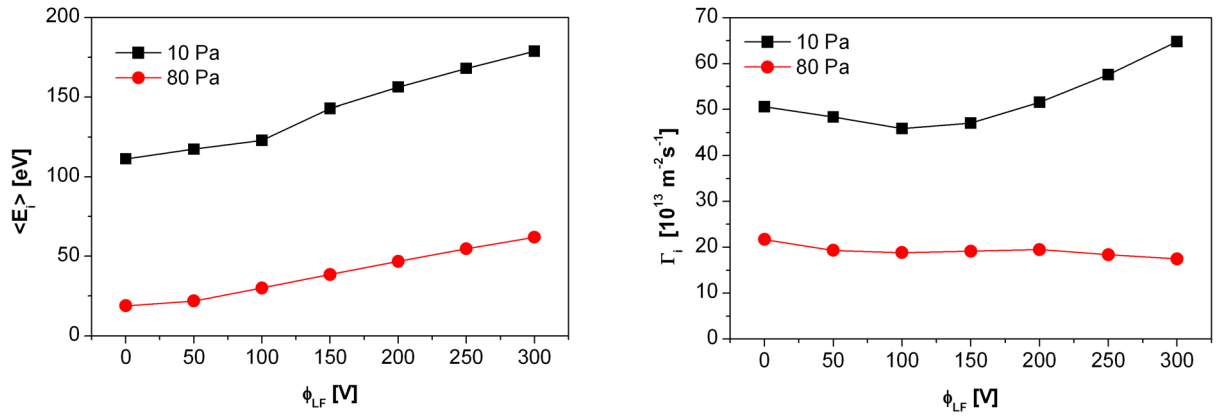

Figure 6: Mean ion energy (left plot), $\langle E_i \rangle$, and ion flux (right plot), Γ_i, at the electrodes in classical dual-frequency discharges as a function of the low-frequency voltage amplitude, Φ_{LF}, at different pressures (10 Pa and 80 Pa). f_{LF} = 1.937 MHz, f_{HF} = 27.12 MHz, Φ_{HF}=300 V at 10 Pa and Φ_{HF}=100 V at 80 Pa.

the low and high frequency current components are in phase.

The electronegativity of the discharge, *i.e.*, the ratio of the spatially and temporally averaged negative ion and electron density, is generally larger under these high pressure conditions. Furthermore, it is significantly affected by the application of a low-frequency source at 80 Pa (Fig. 5): compared to the case of single-frequency excitation (Φ_{LF}=0 V), the electronegativity decreases for high values of Φ_{LF}. This effect can be explained by the impact of Φ_{LF} on the length of the bulk. At Φ_{LF}=0 V the bulk region, where the negative ions are concentrated, is large. An increase in Φ_{LF} results in larger sheaths and shorter bulk length, *i.e.*, the region, where negative ions can be found is shrunk – this causes the electronegativity of the discharge to decrease.

In Fig. 6 the mean energy of CF_3^+ ions, $\langle E_i \rangle$, and their flux, Γ_i, at the electrodes is shown for 10 Pa and 80 Pa as a function of the low-frequency voltage amplitude, Φ_{LF}. The mean ion energy can be controlled by changing Φ_{LF}; the same trends can be observed in the variation of $\langle E_i \rangle$ at both pressures. Increase in Φ_{LF} results in an increase of the mean sheath voltage that causes positively charged ions to arrive at the electrodes with higher energies. At the two different pressures studied here, different behavior of the ion fluxes at the electrodes is found when varying Φ_{LF} (right plot). At 10 Pa, the ion flux at the electrodes decreases as a function of Φ_{LF} for Φ_{LF}<100 V, while it increases for values of Φ_{LF} above 100 V. At this pressure, the discharge operates in the α–mode. The decrease of Γ_i is the consequence of the frequency-coupling mechanism that reduces the electron heating and ionization at the phases when the low-frequency sheath is large. The increase of Γ_i for Φ_{LF}>100 V can be explained by the effect of secondary electrons that are accelerated in the large sheath and can induce significant ionization [50].

At 80 Pa, the discharge operates in a hybrid α–DA mode. Changing Φ_{LF} affects the electron heating due to the high-frequency sheath oscillations as well as the electron heating caused by the high drift and ambipolar electric fields in the discharge center and around the maximum sheath edges, respectively. At low values of Φ_{LF} (<50 V), the decrease of Γ_i is caused by a less efficient α–mode electron heating and ionization. This is due to the fact that the relatively long time scale of the low frequency component allows for a weak dynamics of the negative ion density diffusing into the region of sheaths oscillation. Therefore, fewer electrons are accelerated in the sheaths expansion phases. The overall plasma density (Fig. 4) and the ion flux (Fig. 6) decrease because the loss in the α–mode heating efficiency cannot be compensated by the relatively weak DA-mode heating. At higher values of Φ_{LF} (<200 V), the DA-mode becomes dominant and compensates for the weaker α–mode heating, yielding an almost constant peak of ion density (Fig. 4) and total ion flux (Fig. 6), respectively. Meanwhile, the mean ion energy at the electrodes can be changed by a factor of about 2 by increasing Φ_{LF}. A further increase of Φ_{LF} (>200 V) results in a slight decrease of Γ_i, which can be attributed to the effect of Φ_{LF} on the length of the bulk: at high values of Φ_{LF}, the sheath is large, so that the electron heating in the DA-mode and ionization take place in the short bulk region. In addition, the α–mode heating becomes less effective due to the negative ion dynamics as described above. It should be noted that, in contrast to the 10 Pa case, secondary electrons do not play a significant role, even under high voltage amplitude conditions. There are two reasons for the negligible amount of ionization

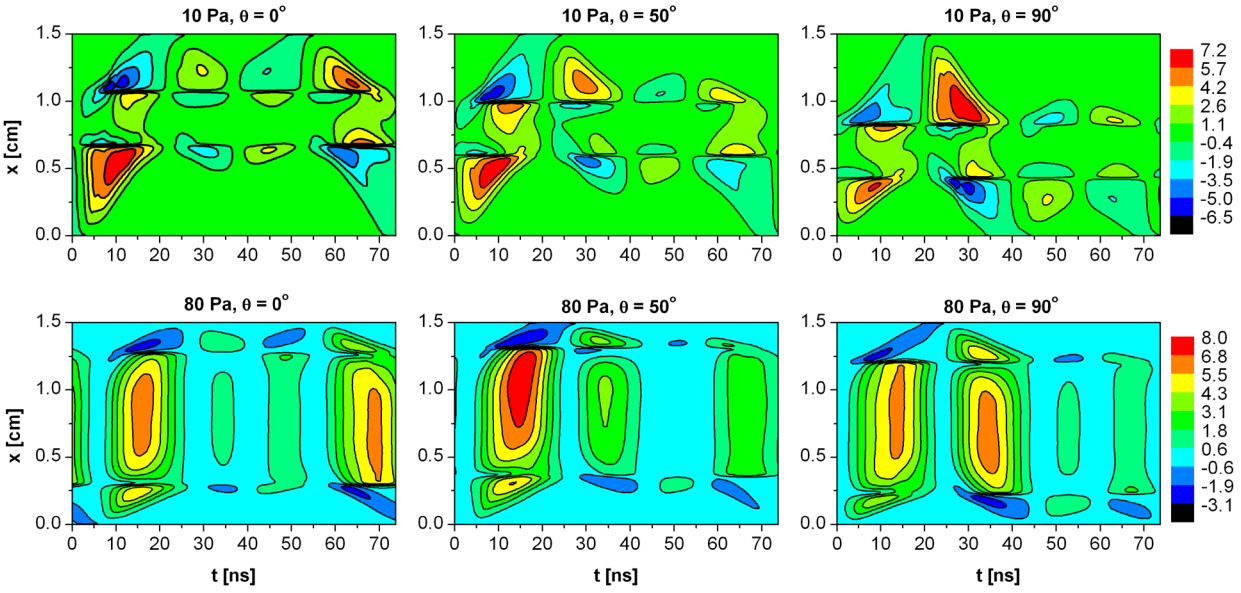

Figure 7: Spatio-temporal distribution of the electron heating rate in electrically asymmetric dual-frequency discharges operated at 13.56 MHz + 27.12 MHz for different values of the phase shift between the driving harmonics, θ, at 10 Pa, $\Phi_{LF}=\Phi_{HF}=100$ V (first row) and at 80 Pa, $\Phi_{LF}=\Phi_{HF}=50$ V (second row). The color scales are given in 10^4 Wm^{-3} and apply to all plots in the same row.

by secondary electrons: Firstly, the ion flux is smaller at higher pressures due to the longer time scale of diffusion in the collisional regime, thereby reducing the amount of electrons released from the electrodes surfaces due to ion impact. Secondly, the reduced electric field in the sheaths is smaller compared to that in the low pressure case. The maximum sheath extensions and maximum voltage drop across each of the sheaths is similar in the dual-frequency high pressure case (80 Pa, Φ_{LF}=100 V, Φ_{HF}=200 V) and in the low pressure single-frequency case (10 Pa, Φ_{LF}=0 V, Φ_{HF}=300 V). During the acceleration in the respective sheaths electric field the electrons undergo too many collisions at 80 Pa – because of the various collision processes in a molecular gas – to allow for an efficient multiplication. Therefore, counterintuitively, secondary electrons can be neglected in the discussion of the electron heating dynamics and ion flux formation at 80 Pa, whereas they explain the increase in the ion flux for the higher voltage amplitudes at 10 Pa.

3.2 Electrically asymmetric dual-frequency discharges

In Fig. 7 spatio-temporal plots of the electron heating rate in electrically asymmetric dual-frequency discharges driven at 13.56 MHz + 27.12 MHz are shown for 10 Pa (first row) and 80 Pa (second row) for different phase shifts between the driving harmonics (first column: θ=0°, second column: θ=50°, third column: θ=90°). Equal and constant voltage amplitudes are set for the low-frequency and high-frequency sources, $\Phi_{LF}=\Phi_{HF}$=100 V at 10 Pa and $\Phi_{LF}=\Phi_{HF}$=50 V at 80 Pa. In Figs. 8 and 9 the spatio-temporal distribution of the ionization rate and electric field corresponding to these cases are shown. In these plots the time axis covers one period of the low-frequency source (73.74 ns). We discuss the effect of the variation of the phase shift between the driving harmonics on the electron heating and ionization dynamics at different pressures, followed by the analysis of the impact of changing θ on the separate control of ion properties at the electrodes.

At 10 Pa, for θ=0°, electron heating at the expanding sheath edge, as well as heating in the bulk region and at the collapsing sheath edge, can be observed (Fig. 7, top left plot). The sheath expansion heating of electrons is stronger than that in the bulk region and at the collapsing sheath edge, but all these heating mechanisms contribute significantly to the ionization (Fig. 8, top left plot), *i.e.*, the discharge operates in a hybrid α-DA mode. The electronegativity of the discharge is 11.7, the density of F^- ions and that of CF_3^- ions are about 36 and 7 times higher, respectively, than the electron density averaged over the discharge gap. A local maximum of the electron density is found (Fig. 10, top left plot) at the position of the transition between the electronegative bulk and electropositive sheath region. By changing θ to 50°, the electronegativity of the discharge slightly increases (up to 12.8). While at θ=0° a strong maximum of the ionization rate is found

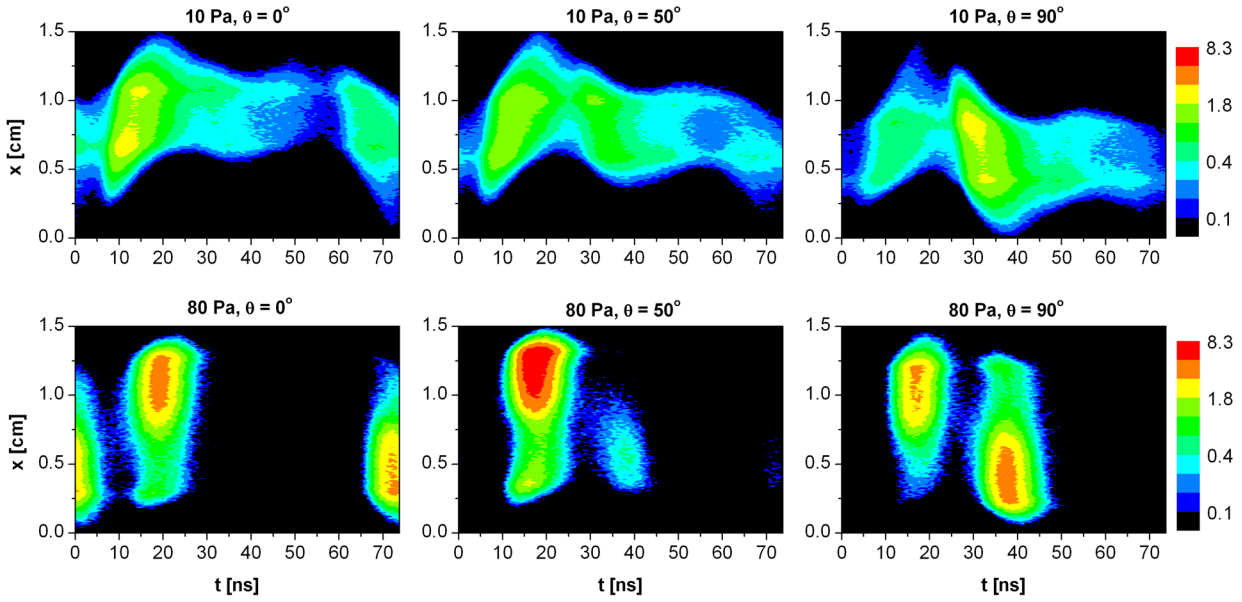

Figure 8: Spatio-temporal distribution of the ionization rate in electrically asymmetric dual-frequency discharges operated at 13.56 MHz + 27.12 MHz for different values of the phase shift between the driving harmonics, θ, at 10 Pa, $\Phi_{LF}=\Phi_{HF}=100$ V (first row) and at 80 Pa, $\Phi_{LF}=\Phi_{HF}=50$ V (second row). The color scales, given in 10^{21} $m^{-3}s^{-1}$, are logarithmic, and apply to all plots in the same row.

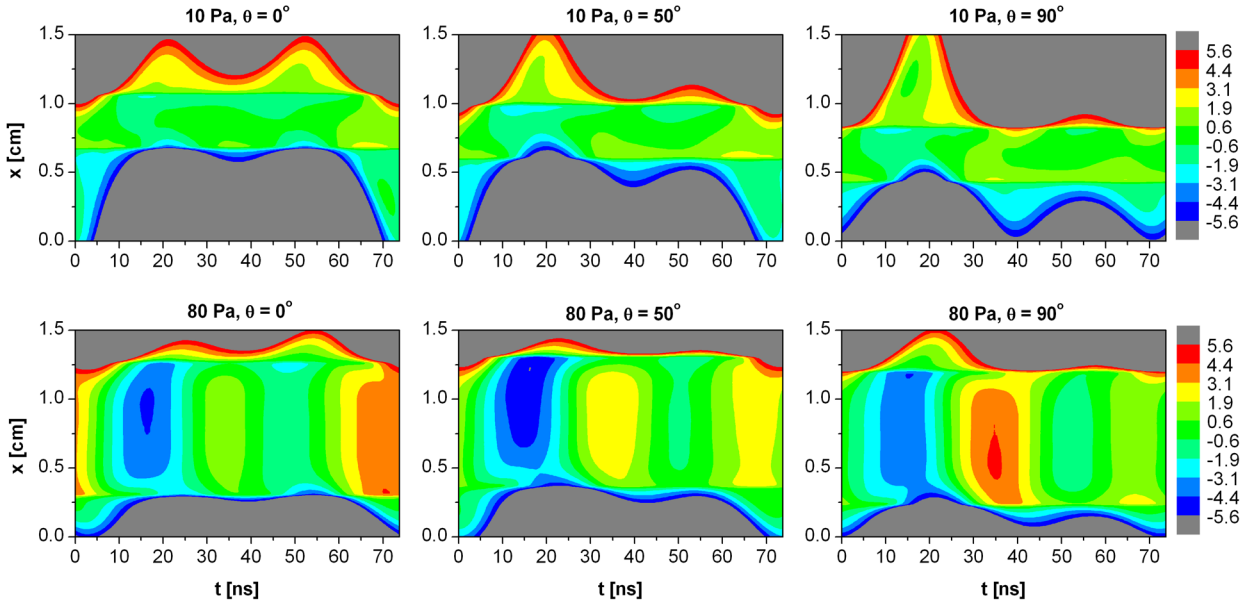

Figure 9: Spatio-temporal distribution of the electric field in electrically asymmetric dual-frequency discharges operated at 13.56 MHz + 27.12 MHz for different values of the phase shift between the driving harmonics, θ, at 10 Pa, $\Phi_{LF}=\Phi_{HF}=100$ V (first row) and at 80 Pa, $\Phi_{LF}=\Phi_{HF}=50$ V (second row). The color scales are given in 10^3 Vm^{-1} and apply to all plots in the same row.

only once within the low-frequency period, for θ=50° two similarly strong maxima of the ionization can be observed within one low-frequency period (Fig. 8, top middle plot). At θ=90° the role of the powered and grounded electrodes is reversed and the ionization dynamics are reversed accordingly compared to the case when θ=0°.

At 80 Pa, the electron heating and ionization in the bulk region dominates over the heating and ionization due to sheath expansion (Fig. 7 and 8, bottom plots) as the discharge is strongly electronegative (the electronegativity is about 45). The electron heating is mainly determined by the drift electric field in the bulk

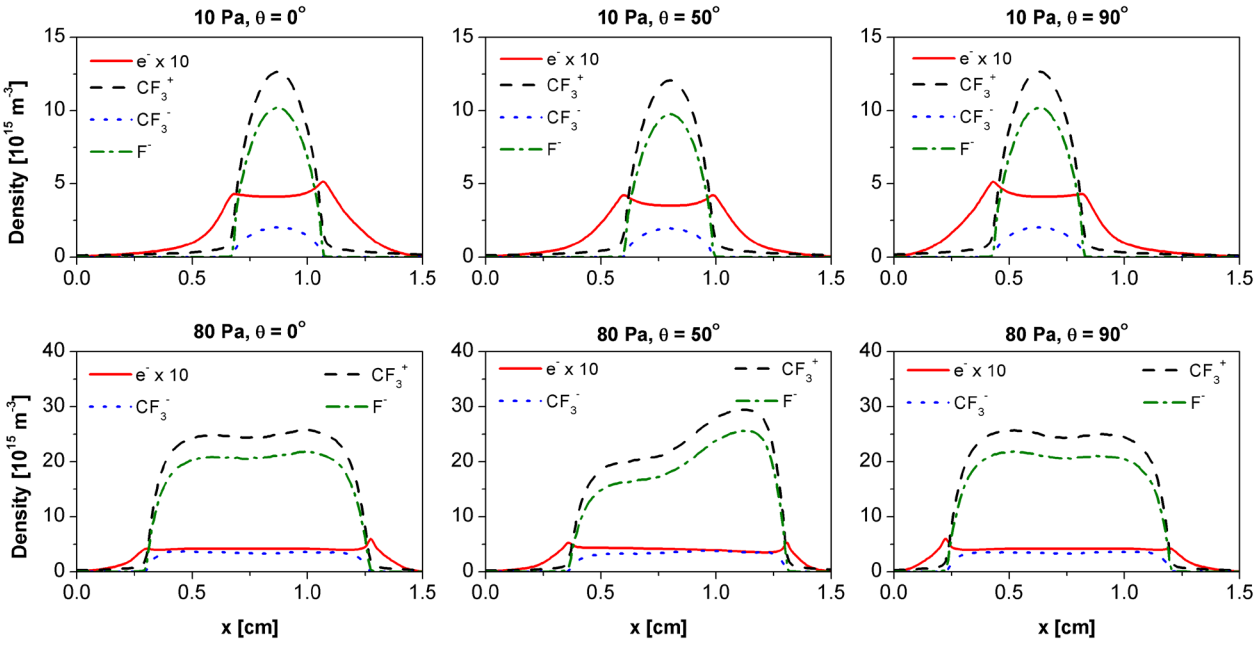

Figure 10: Time averaged charged particle densities in electrically asymmetric dual-frequency discharges operated at 13.56 MHz + 27.12 MHz for different values of the phase shift between the driving harmonics, θ, at 10 Pa, $\Phi_{LF}=\Phi_{HF}$= 100 V (first row) and at 80 Pa, $\Phi_{LF}=\Phi_{HF}$= 50 V (second row). The color scales are given in 10^3 Vm^{-1} and apply to all plots in the same row.

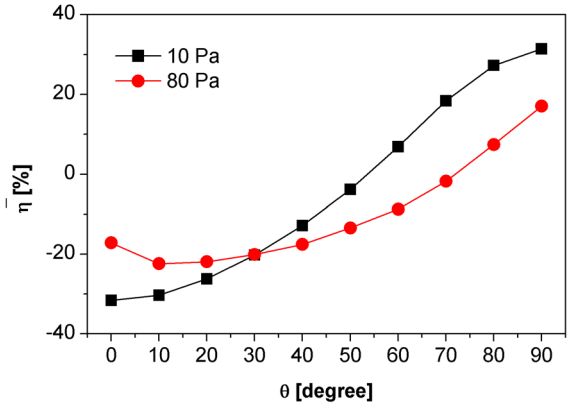

Figure 11: Dc self-bias as a function of θ in electrically asymmetric dual-frequency discharges operated at 13.56 MHz + 27.12 MHz at 10 Pa, $\Phi_{LF}=\Phi_{HF}$= 100 V and at 80 Pa, $\Phi_{LF}=\Phi_{HF}$= 50 V.

(Fig. 9). At θ=0° and θ=90° the electron heating and ionization rates have two similarly strong maxima within a low-frequency period. At these times the electric field is high in the bulk (Fig. 9, bottom left and right plots). This high drift field accelerates the electrons once towards the grounded electrode and once towards the powered electrode. The electric field is almost equally strong at the times of its maximum and its minimum due to the shape of the driving voltage waveforms for these phase shifts [16]. At θ=50° only one maximum can be observed in the electron heating and ionization rates. At this phase the electric field is strong only once per low frequency period (Fig. 9). There are two additional maxima per low frequency period, but their amplitudes are significantly lower compared to the global extremum, so that the drift electric field causes strong acceleration of the electrons towards the grounded electrode once per low frequency period and weaker acceleration towards the powered electron twice per low frequency period.

In Fig. 11 the dc self-bias, η, normalized by the total amplitude of the driving voltage waveform, $\eta/(\Phi_{LF}+\Phi_{HF})$, is shown as a function of the phase shift between the driving harmonics, θ, at the two different pressures studied here, 10 Pa and 80 Pa. At both pressures a dc self-bias is generated due to the EAE and can be controlled by tuning θ. In electropositive discharges, the self-bias voltage can generally be varied over a wide range by changing θ between 0° and 90° and it is an almost linear function of θ. The linear dependence of η on θ is not necessarily valid in electronegative CF_4 plasmas. At 10 Pa (where the discharge operates in a hybrid α–DA mode), the difference is not pronounced, while at 80 Pa (where the discharge operates in a DA mode) significant deviation from a linear dependence can be observed. The origin of this deviation, as it has been clarified by an analytical model of the EAE in [16], is due to the electronegativity of CF_4 discharges and the difference between the mean effective ion densities

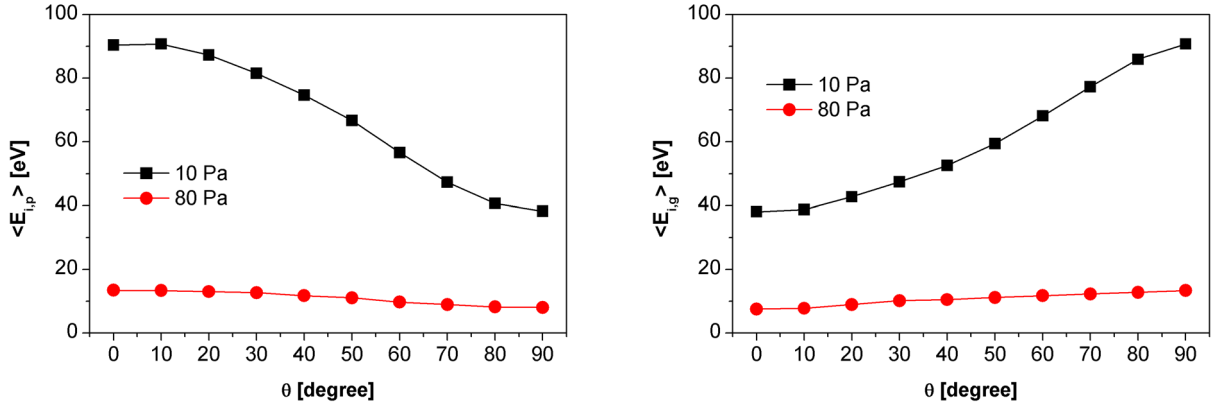

Figure 12: Mean ion energy at the powered (left plot) and grounded (right plot) electrode as a function of θ in electrically asymmetric dual-frequency discharges operated at 13.56 MHz + 27.12 MHz at 10 Pa, $\Phi_{LF}=\Phi_{HF}=100$ V and at 80 Pa, $\Phi_{LF}=\Phi_{HF}=50$ V.

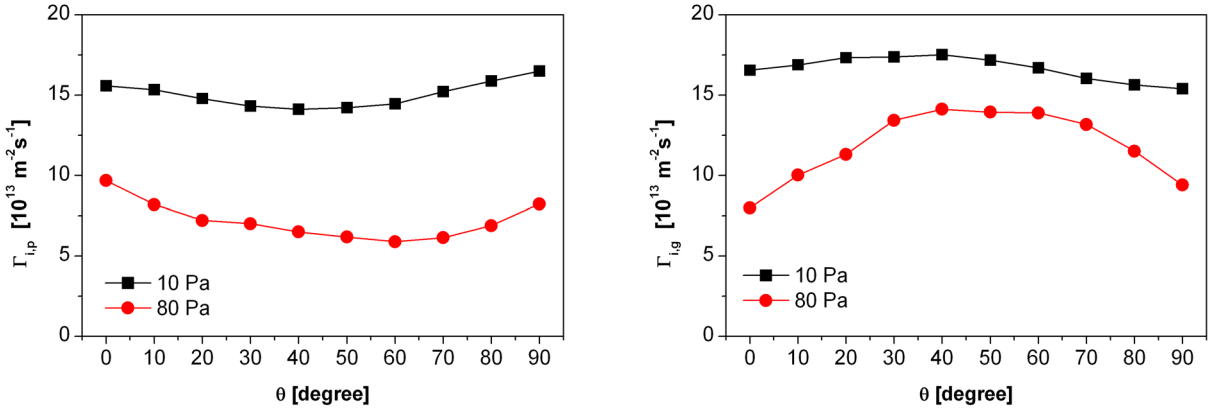

Figure 13: Ion flux at the powered (left plot) and grounded (right plot) electrode as a function of θ in electrically asymmetric dual-frequency discharges operated at 13.56 MHz + 27.12 MHz at 10 Pa, $\Phi_{LF}=\Phi_{HF}=100$ V and at 80 Pa, $\Phi_{LF}=\Phi_{HF}=50$ V.

in both sheaths: The asymmetric ionization profile at θ=50° (Fig. 8) leads to a higher mean positive ion density (Fig. 10) in the grounded sheath compared to the powered one. This asymmetry reduces the dc self-bias value and is the main reason for the difference between both curves shown in Fig. 11. Furthermore, the self-amplification of the EAE at low pressures [54] is very effective at 10 Pa due to the absence of symmetric charge exchange collisions, so that the ion motion within the sheaths is only weakly collisional [16].

In Fig. 12 the mean energy of ions at the powered and grounded electrodes ($\langle E_{i,p}\rangle$ and $\langle E_{i,g}\rangle$, respectively) is shown for 10 Pa and 80 Pa as a function of the phase shift between the driving harmonics, θ. At both pressures, the mean ion energy can be controlled by changing θ at both electrodes; it can be changed by a factor of about 2.4 and 1.75 at 10 Pa and 80 Pa, respectively. At θ=0°, the dc self-bias is strongly negative. Accordingly, the absolute value of the mean sheath voltage is larger at the powered electrode sheath compared to the grounded electrode sheath. This, in turn, leads to $\langle E_{i,p}\rangle$ larger than $\langle E_{i,g}\rangle$, whereas the reverse case is obtained for θ=90°.

The ion fluxes at the powered and grounded electrodes ($\Gamma_{i,p}$ and $\Gamma_{i,g}$, respectively) as a function of θ are shown in Fig. 13. At 10 Pa, the ion flux changes by a factor of maximum 1.2 at both electrodes by tuning θ from 0° and 90°. At 80 Pa, the ion flux at the powered electrode changes by a factor of maximum 1.6, while at the grounded electrode it changes by a factor of maximum 1.8. As discussed above, the discharge is operated in a DA-mode under these high pressure conditions. The asymmetry in the bulk electric field around θ=45° results in a spatially asymmetric ionization profile, as it becomes clear from Fig. 8 (bottom middle plot). Here, the major source of positive ions is located close to the grounded electrode. Therefore, many more ions diffuse to this electrode compared to the powered electrode. This leads to the convex and concave shape of the ion flux dependence on

the phase angle at the powered and the grounded electrode in the range between θ=0° and θ=90°, respectively. Basically, the same tendencies can be observed at lower pressures. However, the α-mode heating contributes significantly to the electron heating and the localization of the ionization is much weaker. Thus, the modulation of the ion flux is less pronounced.

4 Conclusions

We investigated the electron heating and ionization dynamics in classical and electrically asymmetric dual-frequency electronegative CF_4 discharges using PIC/MCC simulations. For both types of discharges the simulation results, obtained for two different pressures while varying the control parameter for the mean ion energy, were analyzed. In classical dual-frequency discharges the low-frequency voltage amplitude, Φ_{LF}, is varied at constant value of the high-frequency voltage amplitude, Φ_{HF}; in electrically asymmetric discharges, the phase shift between the driving harmonics, θ, is changed at constant and equal voltage amplitudes. We analyzed the impact of changing the control parameter on the separate control of ion properties at the electrodes.

We have found that in classical dual-frequency discharges, the discharge is operated in a pure α-mode at low pressures and in a hybrid α-DA mode at higher pressures, respectively. Generally, increasing the voltage amplitude of the low-frequency source has a complex effect on the electron heating and ionization dynamics. At both, a low pressure of 10 Pa and a high pressure of 80 Pa, the α-mode electron heating and ionization is reduced. This can be attributed to the well known frequency-coupling, *i.e.*, the electron heating at times of large low frequency sheath extensions is associated with reduced ionization efficiency. The discharge remains weakly electronegative at 10 Pa, so that the heating by sheath expansion and the acceleration of secondary electrons in the sheaths are the major sources of energetic electrons. At a higher pressure of 80 Pa, the discharge operates in a hybrid α-DA mode. There, additional frequency coupling effects are found to influence the electron heating and ionization dynamics: Applying a low-frequency source strongly reduces the α-mode heating and leads to distinct peaks of the spatio-temporal electron heating by the ambipolar field at the times of in phase low and high frequency currents, which occur only in a fraction of the low frequency period due to the large sheath edge oscillations. The strength of the drift field within the plasma bulk and the subsequent electron heating is alternating according to the current directions of the low and the high frequency components, as well. These mechanisms of electron heating in the DA-mode, which are present only in electronegative and/or dusty plasmas in this pressure regime, can compensate the negative effect of the frequency coupling on the sheath expansion heating. Thereby, the separate control of the mean ion energy and the ion flux at the electrodes can be realized for a narrow parameter window.

In electrically asymmetric dual-frequency discharges, tuning the phase angle θ between the applied frequencies does not lead to a change in the dominant electron heating mode: the discharge is operated in a hybrid α-DA mode at low and high pressures, whereas the α-mode is observed to be stronger at 10 Pa and the DA-mode is observed to be stronger at 80 Pa, respectively. However, tuning θ changes the shape of the driving voltage waveform, thereby leading to complex changes of the electron heating dynamics, again. The electrical generation of a dc self-bias causes the mean ion energies at both electrodes to differ from each other at 0° and 90°, respectively. At high pressures the electron heating is almost symmetric for these phase shifts and the ions flow almost equally to both electrodes. However, in the intermediate phase angle range, the spatio-temporal electron heating dynamics is strongly asymmetric at high pressures. As a consequence, a spatially asymmetric ionization profile develops and the ion flux is no longer evenly distributed among the powered and the grounded electrode. This asymmetry affects the electrical generation of a dc self-bias *via* the electrical asymmetry effect. Furthermore, it leads to a strong limitation of the separate control of ion energy and ion flux in electronegative discharges, particularly under the discharge conditions where the electron heating is dominated by the DA-mode, *e.g.* at relatively high pressures.

Acknowledgments: This work has been supported by the Hungarian Scientific Research Fund through the grant OTKA K-105476.

References

[1] Lieberman M.A., Lichtenberg A.J., Principles of Plasma Discharges and Materials Processing, 2nd edition, Wiley-Interscience, Hoboken, NJ, 2005

[2] Makabe T., Petrović Z.Lj., Plasma Electronics: Applications in Microelectronic Device Fabrication, Taylor and Francis, New York, 2006

[3] Georgieva V., Bogaerts A., Gijbels R., Numerical investigation of ion-energy-distribution functions in single and dual frequency capacitively coupled plasma reactors, Phys. Rev. E, 2004, 69, 026406

[4] Georgieva V., Bogaerts A., Numerical simulation of dual frequency etching reactors: Influence of the external process parameters on the plasma characteristics, J. Appl. Phys., 2005, 98, 023308
[5] Georgieva V., Bogaerts A., Plasma characteristics of an Ar/CF4/N2 discharge in an asymmetric dual frequency reactor: numerical investigation by a PIC/MC model, Plasma Sources Sci. Technol., 2006, 15, 368
[6] Donkó Z., Petrović Z.Lj., Analysis of a Capacitively Coupled Dual-Frequency CF4 Discharge, Japan. J. Appl. Phys., 2006, 45, 8151
[7] Denpoh K., Nanbu K., Self-consistent Particle Simulation of Radio-Frequency CF4 Discharge with Implementation of All Ion-Neutral Reactive Collisions, J. Vac. Sci. Technol. A, 1998, 16, 1201-1206
[8] Denpoh K., Nanbu K., Self-Consistent Particle Simulation of Radio Frequency CF4 Discharge: Effect of Gas Pressure, Japan. J. Appl. Phys., 39, 2804-2808
[9] Booth J.P., Corr C.S., Curley G.A., Jolly J., Guillon J., Foldes T., Fluorine negative ion density measurement in a dual frequency capacitive plasma etch reactor by cavity ring-down spectroscopy, Appl. Phys. Lett., 2006, 88, 151502
[10] Cunge G., Chabert P., Booth J.P., Absolute fluorine atom concentrations in fluorocarbon plasmas determined from CF2 loss kinetics, J. Appl. Phys., 2001, 89, 7750
[11] Booth J.P., Optical and Electrical Diagnostics of Fluorocarbon Plasma Etching Processes, Plasma Sources Sci. Technol., 1999, 8, 249
[12] Booth J.P, Cunge G., Chabert P., Sadeghi N., CFx radical production and loss in a CF4 reactive ion etching plasma: fluorine rich conditions, J. Appl.Phys., 1999, 85, 3097
[13] Haverlag M., Kono A., Passchier D., Kroesen G.M.W., Goedheer W.J., de Hoog F.J., Measurements of negative ion densities in 13.56-MHz rf plasmas of CF4, C2F6, CHF3, and C3F8 using microwave resonance and the photodetachment effect, J. Appl. Phys., 1991, 70, 3472
[14] Sobolewski M.A., Wang Y., Goyette A., Measurements and modeling of ion energy distributions in high-density radio-frequency biased CF4 discharges, J. Appl. Phys., 2002, 91, 6303-6314
[15] Proshina O.V., Rakhimova T.V., Rakhimov A.T., Voloshin D.G., Two modes of capacitively coupled rf discharge in CF4, Plasma Sources Sci. Technol., 2010, 19, 065013
[16] Schulze J., Derzsi A., Donkó Z., Electron heating and the electrical asymmetry effect in dual-frequency capacitive CF4 discharges, Plasma Sources Sci. Technol., 2011, 20, 045008
[17] Schulze J., Derzsi A., Dittmann K., Hemke T., Meichsner J., Donkó Z., Ionization by Drift and Ambipolar Electric Fields in Electronegative Capacitive Radio Frequency Plasmas, Phys. Rev. Lett., 2011, 107, 275001
[18] Derzsi A., Donkó Z., Schulze J., Coupling effects of driving frequencies on the electron heating in electronegative capacitive dual-frequency plasmas, J. Phys. D: Appl. Phys., 2013, 46, 482001
[19] Teichmann T., Küllig C., Dittmann K., Matyash K., Schneider R., Meichsner J., Particle-In-Cell simulation of laser photodetachment in capacitively coupled radio frequency oxygen discharges, Phys. Plasmas, 2013, 20, 113509
[20] Dittmann K., Küllig C., Meichsner J, Electron and negative ion dynamics in electronegative cc-rf plasmas, Plasma Phys. Control. Fusion, 2012, 54, 124038
[21] Belenguer P., Boeuf J.P., Transition between different regimes of rf glow discharges, Phys. Rev. A, 1990, 41, 4447
[22] Vender D., Boswell R., Electron–sheath interaction in capacitive radio-frequency plasmas, J. Vac. Sci. Technol. A, 1992, 10, 1331
[23] Schulze J., Heil B.G., Luggenhölscher D., Mussenbrock T., Brinkmann R.P., Czarnetzki U., Electron beams in asymmetric capacitively coupled radio frequency discharges at low pressures, J. Phys. D: Appl. Phys., 2008, 41, 042003
[24] Turner M.M., Hopkins M.B., Anomalous sheath heating in a low pressure rf discharge in nitrogen, Phys. Rev. Lett., 1992, 69, 3511
[25] Czarnetzki U., Luggenhölscher D., Döbele H.F., Space and time resolved electric field measurements in helium and hydrogen RF-discharges, Plasma Sources Sci. Technol., 1999, 8, 230
[26] Schulze J., Donkó Z., Heil B.G., Luggenhölscher D., Mussenbrock T., Brinkmann R.P., et al., Electric field reversals in the sheath region of capacitively coupled radio frequency discharges at different pressures, J. Phys. D: Appl. Phys., 2008, 41, 105214
[27] Hemke T., Eremin D., Mussenbrock T., Derzsi A., Donkó Z., Dittmann K., et al., Ionization by bulk heating of electrons in capacitive radio frequency atmospheric pressure microplasmas, Plasma Sources Sci. Technol., 2013, 22, 015012
[28] Belenguer P., Blondeau J.P, Boufendi L., Toogood M, Plain A., Bouchoule A, et al., Phys. Rev. A, 1992, 46, 7923
[29] Schüngel E., Mohr S., Iwashita S., Schulze J., Czarnetzki U., The effect of dust on electron heating and dc self-bias in hydrogen diluted silane discharges, J. Phys. D: Appl. Phys., 2013, 46, 175205
[30] Killer E., Bandelow G., Matyash K., Schneider R., Melzer A., Observation of Ω Mode Electron Heating in dusty argon radio frequency discharges, Phys. Plasmas, 2013, 20, 083704
[31] Shibata M., Nakano N., Makabe T., O2 rf discharge structure in parallel plates reactor at 13.56 MHz for material processing, J. Appl. Phys., 1995, 77, 6181
[32] Liu Y.X., Zhang Q.Z., Liu J., Song Y.H., Bogaerts A., Wang Y.N., Effect of bulk electric field reversal on the bounce resonance heating in dual-frequency capacitively coupled electronegative plasmas, Appl. Phys. Lett., 2012, 101, 114101
[33] Liu Y.X., Zhang Q.Z., Liu J., Song Y.H., Bogaerts A., Wang Y.N., Electron bounce resonance heating in dual-frequency capacitively coupled oxygen discharges, Plasma Sources Sci. Technol., 2013, 22, 025012
[34] Yan M., Bogaerts A., Goedheer W.J., Gijbels R., Electron energy distribution function in capacitively coupled RF discharges: difference between electropositive Ar and electronegative SiH4 discharges, Plasma Sources Sci. Technol., 2000, 9, 583
[35] Jiang W., Xu X., Dai Z.L., Wang Y.N., Heating mechanisms and particle flow balancing of capacitively coupled plasmas driven by combined dc/rf sources, Phys. Plasmas, 2008, 15, 033502
[36] Wang S.B., Wendt A.E., Control of ion energy distribution at substrates during plasma processing, J. Appl. Phys., 2000, 88, 643
[37] Qin X.V., Ting Y.H., Wendt A.E., Tailored ion energy distributions at an rf-biased plasma electrode, Plasma Sources Sci. Technol., 2010, 19, 065014
[38] Rauf S., Kushner M.J., Nonlinear dynamics of radio frequency plasma processing reactors powered by multifrequency sources, IEEE Trans. Plasma Sci., 1999, 27, 1329-1338
[39] Schulze J., Schüngel E., Czarnetzki U., Coupling effects in inductive discharges with radio frequency substrate biasing, Appl. Phys. Lett., 2012, 100, 024102

[40] Lee H.C., Lee M.H., Chung C.W., Effects of rf-bias power on plasma parameters in a low gas pressure inductively coupled plasma, Appl. Phys. Lett., 2010, 96, 071501

[41] Lee H.C., Chung C.W., Collisionless electron heating by radio frequency bias in low gas pressure inductive discharge, Appl. Phys. Lett., 2012, 101, 244104

[42] Boyle P.C., Ellingboe A.R., Turner M.M., Independent control of ion current and ion impact energy onto electrodes in dual frequency plasma devices, J. Phys. D: Appl. Phys., 2004, 37, 697

[43] Kitajima T., Takeo Y., Petrović Z.Lj., Makabe T., Functional separation of biasing and sustaining voltages in two-frequency capacitively coupled plasma, Appl. Phys. Lett., 2000, 77, 489

[44] Denda T., Miyoshi Y., Komukai Y., Goto T., Petrović Z.Lj., Makabe T., Functional separation in two frequency operation of an inductively coupled plasma, J. Appl. Phys., 2004, 95, 870

[45] Lee J.K., Manuilenko O.V., Babaeva N.Y., Kim H.C., Shon J.W., Ion energy distribution control in single and dual frequency capacitive plasma sources, Plasma Sources Sci. Technol., 2005, 14, 89

[46] Gans T., Schulze J., O'Connell D., Czarnetzki U., Faulkner R., Ellingboe A.R. et al., Frequency coupling in dual frequency capacitively coupled radio-frequency plasmas, Appl. Phys. Lett., 2006, 89, 261502

[47] Turner M.M., Chabert P., Collisionless Heating in Capacitive Discharges Enhanced by Dual-Frequency Excitation, Phys. Rev. Lett., 2006, 96, 205001

[48] Schulze J., Gans T., O'Connell D., Czarnetzki U., Ellingboe A.R., Turner M.M., Space and phase resolved plasma parameters in an industrial dual-frequency capacitively coupled radio-frequency discharge, J. Phys. D: Appl. Phys., 2007, 40, 7008

[49] Donkó Z., In: J. Matuska, S. Matejcik, J.D. Skalny (Eds.), Modeling of Dual-Frequency Capacitive Discharges, Proceedings of Symposium of Application of Plasma Processes (20–25 January 2007, Podbanske, Slovakia), 2007, IL 02 21–24

[50] Donkó Z., Schulze J., Hartmann P., Korolov I., Czarnetzki U., Schüngel E., The effect of secondary electrons on the separate control of ion energy and flux in dual-frequency capacitively coupled radio frequency discharges, Appl. Phys. Lett., 2010, 97, 081501

[51] Booth J.P., Curley G., Marić D., Chabert P., Dual-frequency capacitive radiofrequency discharges: effect of low-frequency power on electron density and ion flux, Plasma Sources Sci. Technol., 2010, 19, 015005

[52] Schulze J., Donkó Z., Schüngel E., Czarnetzki U., Secondary electrons in dual-frequency capacitive radio frequency discharges, Plasma Sources Sci. Technol., 2011, 20, 045007

[53] Heil B.G., Schulze J., Mussenbrock T., Brinkmann R.P., Czarnetzki U., Numerical Modeling of Electron Beams Accelerated by the Radio Frequency Boundary Sheath, IEEE Trans. Plasma Sci., 2008, 36, 1404-1405

[54] Heil B.G., Czarnetzki U., Brinkmann R.P., Mussenbrock T., On the possibility of making a geometrically symmetric RF-CCP discharge electrically asymmetric, J. Phys. D: Appl. Phys., 2008, 41, 165202

[55] Donkó Z., Schulze J., Heil B.G., Czarnetzki U., PIC simulations of the separate control of ion flux and energy in CCRF discharges via the electrical asymmetry effect, J. Phys. D: Appl. Phys., 2008, 42, 025205

[56] Czarnetzki U., Heil B.G., Schulze J., Donkó Z., Mussenbrock T., Brinkmann R.P., The Electrical Asymmetry Effect - A novel and simple method for separate control of ion energy and flux in capacitively coupled RF discharges, J. Phys. Conf. Ser., 2009, 162, 012010

[57] Schulze J., Schüngel E., Donkó Z., Czarnetzki U., The electrical asymmetry effect in capacitively coupled radio frequency discharges – measurements of dc self bias, ion energy and ion flux, J. Phys. D: Appl. Phys., 2009, 42, 092005

[58] Donkó Z., Schulze J., Czarnetzki U., Luggenhölscher D., Self-excited nonlinear plasma series resonance oscillations in geometrically symmetric capacitively coupled radio frequency discharges, Appl. Phys. Lett., 2009, 94, 131501

[59] Longo S., Diomede P., Modeling of Capacitively Coupled RF Plasmas in H2, Plasma Process. Polym., 2009, 6, 370-379

[60] Schulze J., Schüngel E., Donkó Z., Czarnetzki U., Optimization of the electrical asymmetry effect in dual-frequency capacitively coupled radio frequency discharges: Experiment, simulation, and model, J. Appl. Phys., 2009, 106, 063307

[61] Schulze J., Schüngel E., Donkó Z., Czarnetzki U., Excitation dynamics in electrically asymmetric capacitively coupled radio frequency discharges: experiment, simulation, and model, Plasma Sources Sci. Technol., 2010, 19, 045028

[62] Schulze J., Schüngel E., Donkó Z., Czarnetzki U., Charge dynamics in capacitively coupled radio frequency discharges, J. Phys. D: Appl. Phys., 2010, 43, 225201

[63] Zhang Q.Z., Jiang W.J., Hou L.J., Wang Y.N., Numerical simulations of electrical asymmetry effect on electronegative plasmas in capacitively coupled rf discharge, J. Appl. Phys., 2011, 109, 013308

[64] Schulze J., Schüngel E., Donkó Z., Czarnetzki U., The electrical asymmetry effect in multi-frequency capacitively coupled radio frequency discharges, Plasma Sources Sci. Technol., 2011, 20, 015017

[65] Czarnetzki U., Schulze J., Schüngel E., Donkó Z., The electrical asymmetry effect in capacitively coupled radio-frequency discharges, Plasma Sources Sci. Technol., 2011, 20, 024010

[66] Bienholz S., Stymoll T., Awakowitz P., On the electrical asymmetry effect in large area multiple frequency capacitively coupled plasmas, J. Phys. D: Appl. Phys., 2014, 47, 065201

[67] Lafleur T., Delattre P.A., Johnson E.V., Booth J.P., Separate control of the ion flux and ion energy in capacitively coupled radio-frequency discharges using voltage waveform tailoring, Appl. Phys. Lett., 2012, 101, 124104

[68] Lafleur T., Booth J.P., Control of the ion flux and ion energy in CCP discharges using non-sinusoidal voltage waveforms, J. Phys. D, 2012, 45, 395203

[69] Lafleur T., Boswell R. W., Booth J.P., Enhanced sheath heating in capacitively coupled discharges due to non-sinusoidal voltage waveforms, Appl. Phys. Lett., 2012, 100, 194101

[70] Delattre P.A., Lafleur T., Johnson E., Booth J.P., Radio-frequency capacitively coupled plasmas excited by tailored voltage waveforms: comparison of experiment and particle-in-cell simulations, J. Phys. D, 2013, 46, 235201

[71] Kollath R., In: S. Flugge (Ed.), Encyclopedia of Physics, vol. XXI, Springer, Berlin, 1956

[72] Kurihara M., Petrović Z.Lj., Makabe T., Transport coefficients and scattering cross-sections for plasma modelling in CF4-Ar mixtures: a swarm analysis, J. Phys. D: Appl. Phys., 2000, 33, 2146

[73] Dujko S., Raspopovic Z.M., Petrović Z.Lj., Monte Carlo studies of electron transport in crossed electric and magnetic fields in CF4, J. Phys. D: Appl. Phys., 2005, 38, 2952

[74] Bonham R.A., Electron Impact Cross Section Data for Carbon Tetrafluoride, Japan. J. Appl. Phys., 1994, 33, 4157
[75] Nanbu K., Probability theory of electron-molecule, ion-molecule, molecule-molecule, and Coulomb collisions for particle modeling of materials processing plasmas and cases, IEEE Trans. Plasma Sci., 2000, 28, 971-990
[76] Nanbu K., Kitatani Y., An ion-neutral species collision model for particle simulation of glow discharge, J. Phys. D: Appl. Phys., 1995, 28, 324
[77] Nanbu K., Denpoh K., Monte Carlo Collision Simulation of Positive-Negative Ion Recombination for a Given Rate Constant, J. Phys. Soc. Japan, 1997, 67, 1288-1290